Engineering Structures 265 (2022) 114457

Contents lists available at ScienceDirect

Engineering Structures

journal homepage: www.elsevier.com/locate/engstruct

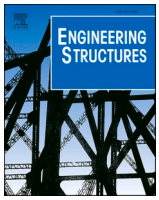

Design, fabrication and analysis of a bio-based tensegrity structure using non-destructive testing

Nathalia B. de Albuquerque [a], Cássio M.R. Gaspar [a,*], Mario Seixas [b,c], Murillo V.B. Santana [d], Daniel C.T. Cardoso [a]

[a] Department of Civil and Environmental Engineering, Pontifical Catholic University of Rio de Janeiro (PUC-Rio), Rua Marquês de São Vicente, 225, Gávea, Rio de Janeiro, RJ 22451-900, Brazil
[b] Department of Arts and Design, Pontifical Catholic University of Rio de Janeiro (PUC-Rio), Rua Marquês de São Vicente, 225, Gávea, Rio de Janeiro, RJ 22451-900, Brazil
[c] Bambutec Design, Rio de Janeiro, Brazil
[d] Institut National des Sciences Appliquées de Rennes, 20 Avenue des Buttes de Coesnes, Rennes, France

ARTICLE INFO

Keywords:
Tensegrity
Bio-based materials
Bamboo
Sisal
Experimental dynamic analysis
Experimental static analysis
Non-destructive testing

ABSTRACT

In this work, an experimental and numerical study of the behavior of a tensegrity structure constructed with natural materials is presented. Firstly, it is shown the concept of tensegrity structures, highlighting its emergence, current context, and applications within Civil Engineering. The design of a bio-based tensegrity structural module is investigated as object of study. Initially, a prototype of a single module of the structure is built in 1:25 scale. Subsequently, a prototype on a 1:5.65 scale is built using *Phyllostachys aurea* bamboo culms for the struts and sisal (*Agave sisalana*) ropes for the cable nets. Both non-destructive static and dynamic testing were performed on the module to investigate the level of prestress right after assembly of the structure and also considering the relaxation of the cable networks under laboratory conditions. The results obtained from the experimental tests are compared with the numerical predictions by means of a relative error parameter regarding the static stresses and the natural frequencies. Thus, it was possible to indirectly determine the level of prestress applied in the sisal ropes of the tensegrity module. The prestress level was equal to 15% in both static and dynamic approaches, which indicates a good agreement between them and points to the robustness of the proposed methodology. The use of bamboo as a suitable material for strut-cord joints is proposed to avoid metal components and consider the end-of-life biodegradability of the structure in the design of joints. The study deploys bio-based materials for tensegrity structures and the kit of parts as a whole, contributing to the development of extremely lightweight and sustainable structural systems.

1. Introduction

According to Motro, a tensegrity system is a stable self-equilibrated state comprising a discontinuous set of compressed components inside a continuum of tensioned components [1]. Tensegrity structures were first idealized and designed by the artist K. Snelson in the 1940s [2,3], however the terminology "tensegrity" was introduced by R.B. Fuller in the 60s as a contraction of the terms "tensile" and "integrity" [4]. Tensegrity structures operate with two types of elements: cable nets – which bear tensile stresses – and struts – that sustain compressive stresses. Furthermore, they are classified as spatial, pin-jointed, lightweight and modular structures where stability and stiffness are obtained by a self-stress state of equilibrium, i.e., cables and struts are loaded by initial forces which provide a stable configuration for the system [1,5].

Tensegrity systems are recognized by their aesthetics, but also by their lightweight and notable load-bearing capacity-to-weight ratio achieved with intelligent employment of building materials. These characteristics have slowly drawn the attention of structural engineers and current applications can be seen in domes, towers, roofs, temporary structures and exhibition pavilions [6–10]. Regarding tensegrity bridges, numerous projects have also been proposed, such as the Tor Vergata footbridge [11], the "Tensegrity Bridge" developed by the firms WilkinsonEyre and Arup for the National Building Museum in Washington, DC [12,13]; and the suspended tensegrity bridge proposed by

* Corresponding author.
E-mail address: cassiogaspar@esp.puc-rio.br (C.M.R. Gaspar).

https://doi.org/10.1016/j.engstruct.2022.114457
Received 9 February 2022; Received in revised form 30 April 2022; Accepted 21 May 2022

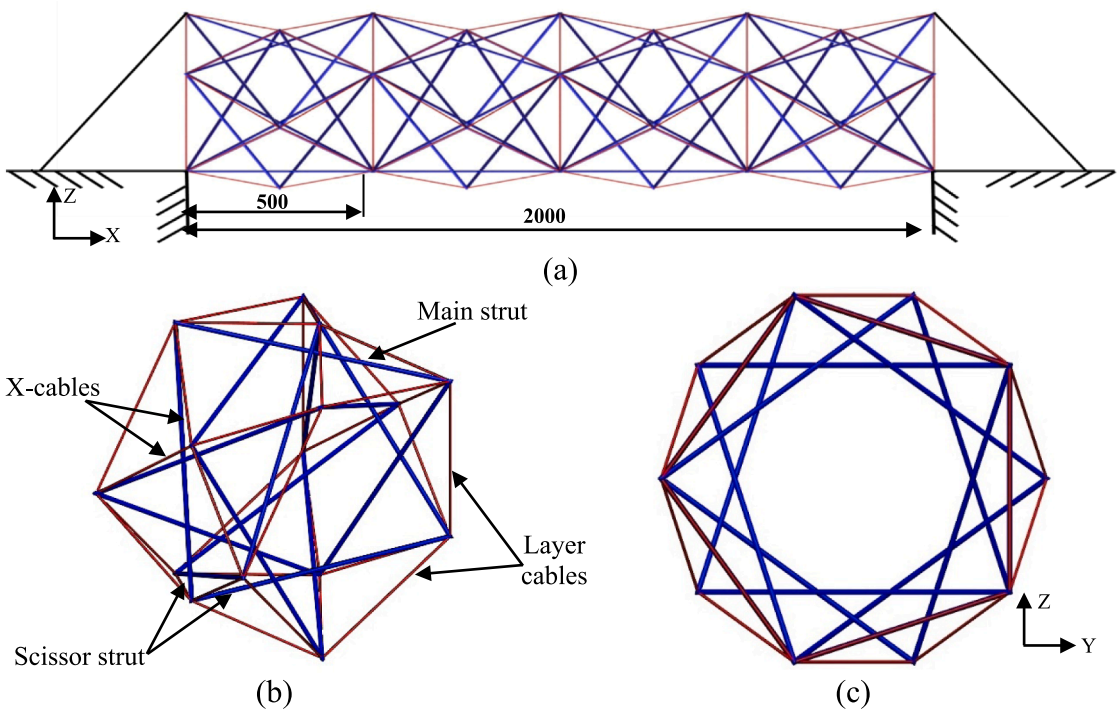

Fig. 1. Pentagonal tensegrity footbridge [15,32]: (a) elevation (side view, dimensions in cm); (b) isometric view of a typical pentagon module; (c) cross-section.

Table 1
Nodal coordinates of a single full-scale module [15].

Node	x (cm)	y (cm)	z (cm)
1	0.00	0.00	389.40
2	0.00	370.30	120.30
3	0.00	228.90	−315.00
4	0.00	−228.90	−315.00
5	0.00	−370.30	120.30
6	250.00	0.00	−389.40
7	250.00	−370.30	−120.30
8	250.00	−228.90	315.00
9	250.00	228.90	315.00
10	250.00	370.30	−120.30
11	500.00	0.00	389.40
12	500.00	370.30	120.30
13	500.00	228.90	−315.00
14	500.00	−228.90	−315.00
15	500.00	−370.30	120.30

Table 2
Connectivity of members [15].

Element	Node	Node	Type	Element	Node	Node	Type
1	1	2	L-cable	24	14	7	X-cable
2	2	3	L-cable	25	5	7	X-cable
3	3	4	L-cable	26	15	7	X-cable
4	4	5	L-cable	27	5	8	X-cable
5	5	1	L-cable	28	15	8	X-cable
6	11	12	L-cable	29	1	8	X-cable
7	12	13	L-cable	30	11	8	X-cable
8	13	14	L-cable	31	1	12	Main strut
9	14	15	L-cable	32	2	13	Main strut
10	15	11	L-cable	33	3	14	Main strut
11	1	9	X-cable	34	4	15	Main strut
12	11	9	X-cable	35	5	11	Main strut
13	2	9	X-cable	36	15	9	Scissor strut
14	12	9	X-cable	37	9	3	Scissor strut
15	2	10	X-cable	38	11	10	Scissor strut
16	12	10	X-cable	39	10	4	Scissor strut
17	3	10	X-cable	40	12	6	Scissor strut
18	13	10	X-cable	41	6	5	Scissor strut
19	3	6	X-cable	42	13	7	Scissor strut
20	13	6	X-cable	43	7	1	Scissor strut
21	4	6	X-cable	44	14	8	Scissor strut
22	14	6	X-cable	45	8	2	Scissor strut
23	4	7	X-cable				

Mucedola and Paradiso to Sesia River in Italy [12]. An existing footbridge based on the tensegrity principle can be seen in Brisbane, Australia: the Kurilpa Bridge is a 470-m-long pedestrian bridge built in 2009 [14]. Within the body of knowledge regarding tensegrity structures, there is a specific family of tensegrity modules called "tensegrity rings" that can be assembled in a "hollow rope" system. This concept shows a strong aptitude for footbridges as demonstrated by Rhode-Barbarigos et al. [15,16], by assembling elementary tensegrity modules. Gao, Xu & Luo [13] recapitulated past studies on "hollow rope" pedestrian bridges, identified unclear aspects and suggested a novel understanding on the tensegrity footbridges based on ring modules, including a new structural efficiency index.

Many authors have made significant contributions regarding both structural static and dynamic behavior, since tensegrity structures exhibit a nonlinear behavior when subjected to external forces and can experience large displacements. Such nonlinearity is due to its flexibility, which implies a change in the stiffness of the structural system as a result of nodal displacements [1]. Ali et al. [17] stated that the self-stress is necessary for stabilizing the tensegrity structure by activating

Table 3
Geometry and mechanical parameters of the bamboo struts and sisal cables.

Element	Parameters (Mean values)	Value
Bamboo strut	Outer diameter (mm)	29.30
	Thickness (mm)	3.80
	Length (cm)	120.00
	Elastic modulus (GPa)	19.40
	Compressive strength (MPa)	68.80
	Specific mass (kg/m^3)	840.15
Sisal cable	Nominal diameter (mm)	6.00
	Length layer cables (cm)	81.00
	Length X-cables (cm)	61.40
	Elastic modulus (GPa)	1.05
	Tensile strength (MPa)	79.60
	Specific mass (kg/m^3)	983.00

the geometrical stiffness. In fact, the equilibrium between tensile and compressive forces is responsible for the structural stability and ultimately for the load bearing capacity of tensegrity structures. Kebiche et al. [18] applied a calculation method previously developed for structures with large deformations and displacements to investigate the behavior of tensegrity structures under static loads of tension, compression, bending and torsion. The authors noted that, except for compression, the structure stiffens as loading increases. Still on static loading, Kahla and Kebiche [19] introduced a procedure for nonlinear elastoplastic analysis using updated Lagrangian formulation and modified Newton-Raphson method. Tran and Lee [20] also used Lagrangian formulations to present a numerical method to analyze large deflections including geometric and material nonlinearity. The results show that forces and displacements are highly influenced by span size and prestress levels. Lagrangians are also often used for dynamic analysis of tensegrities. Murakami investigated the elastic behavior of a cylindrical tensegrity, concluding that the static and dynamic response of tensegrity structures are characterized by infinitesimal mechanism modes and prestresses [21].

In their studying proposing tensegrity modules for a pedestrian bridges, Rhode-Barbarigos et al. [22] showed that the structural behavior is greatly influenced by different levels of prestress applied to the structure. Ashwear and Eriksson studied the effect of the prestress level on the natural frequencies of the tensegrity structure using Euler–Bernoulli beam elements, which include the effect of axial force on stiffness [23]. Vibration modes show that when the force on the compressed elements approaches the critical buckling load, the tensegrity has lower vibration frequencies. Faroughi and Tur [24] developed an algorithm that finds the optimal values of the design parameters, such as the prestress force and the cross-sectional area of the elements that satisfy the desired vibrational properties for the structure. The final values are accepted when the design conditions – such as restraints to buckling and ultimate strength of the elements – are fully satisfied. Ashwear and Eriksson [25] discussed how to design tensegrities to make them viable for vibration monitoring methods. According to the authors, the pattern and the prestress level are important parameters that affect the stiffness and dynamics of tensegrity structures. Over time, however, the design setting can be changed by different factors, such as environmental aspects or external loads. The results show that different prestress losses affect the first vibration mode of the structure differently [25].

In general, the practical applications of tensegrity systems in Civil Engineering are still very limited when compared to traditional structural systems, which can be attributed to their unique structural behavior and complex constructional methodology. Moreover, most existing tensegrity structures are made of metallic cables and struts. Besides, it should be noted that many studies related to geometry and form-finding have been published. Recently, Chen et al. [26] suggested an improved form-finding method for tensegrity structures using blocks of the symmetry-adapted force density matrix and Chen et al. [27] studied symmetry representations and elastic redundancy for members of tensegrity structures. However, few researches have focused on the design and construction of tensegrity structures. Nevertheless, applications with natural materials such as bamboo struts have gained attention lately regarding their constructability, connections and structural performance [10,28]. In this sense, blending the tensegrity system with the use of non-conventional materials, the main novelty of this paper concerns the development of “hollow rope” deployable tensegrity modules that can be fabricated using local natural resources and simple and accessible tools.

The study focused on the design, fabrication and self-stress state analysis of a bio-based tensegrity structure developed on non-destructive approaches, namely through static and dynamic testing. Accordingly, a prototype of a single tensegrity module built in 1:25 scale is initially presented in Section 2. This is followed by the step-by-step assembly, mechanical properties and constructional aspects of a reduced-scale tensegrity module (1:5.65) made with bio-based materials such as bamboo struts and sisal ropes, intending to be fully handcrafted for temporary uses. These structures may be applied, for instance, to build temporary footbridges to mitigate the consequences of natural hazards and the main advantages include the use of local natural resources, ease of manufacturing, transportation, and quick deployment capacity. Section 3 addresses the description and assumptions of the numerical model encompassing the instrumentation procedures of the experimental static and dynamic tests. Considering the hand-made nature of the structure and using the results of the computational model as a reference, Section 4 focuses on both numerical and experimental data in terms of strains, stresses and natural frequencies as alternative procedures to obtain indirect in situ evaluation of the prestress level of the

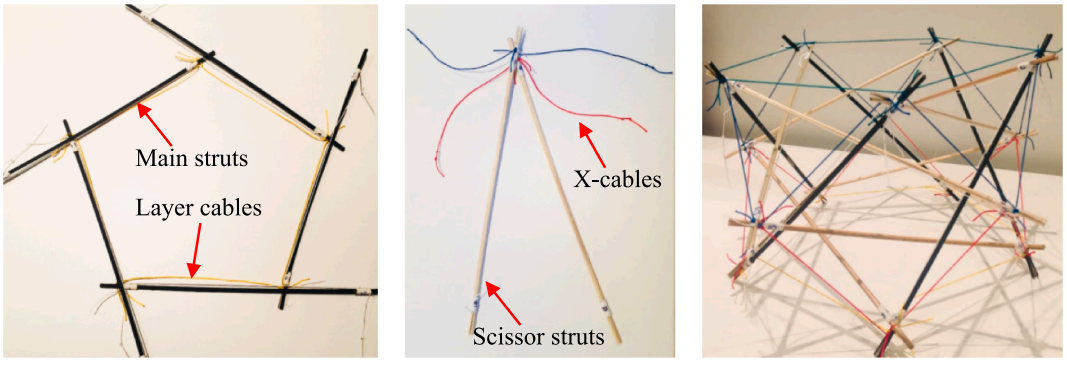

Fig. 2. Small model of a tensegrity structure in 1:25 scale using bamboo sticks and synthetic strings: (a) Superior view of the pentagon formed by the main struts and layer cables; (b) detail of the scissor struts and x-cables; (c) perspective of the module after assembly.

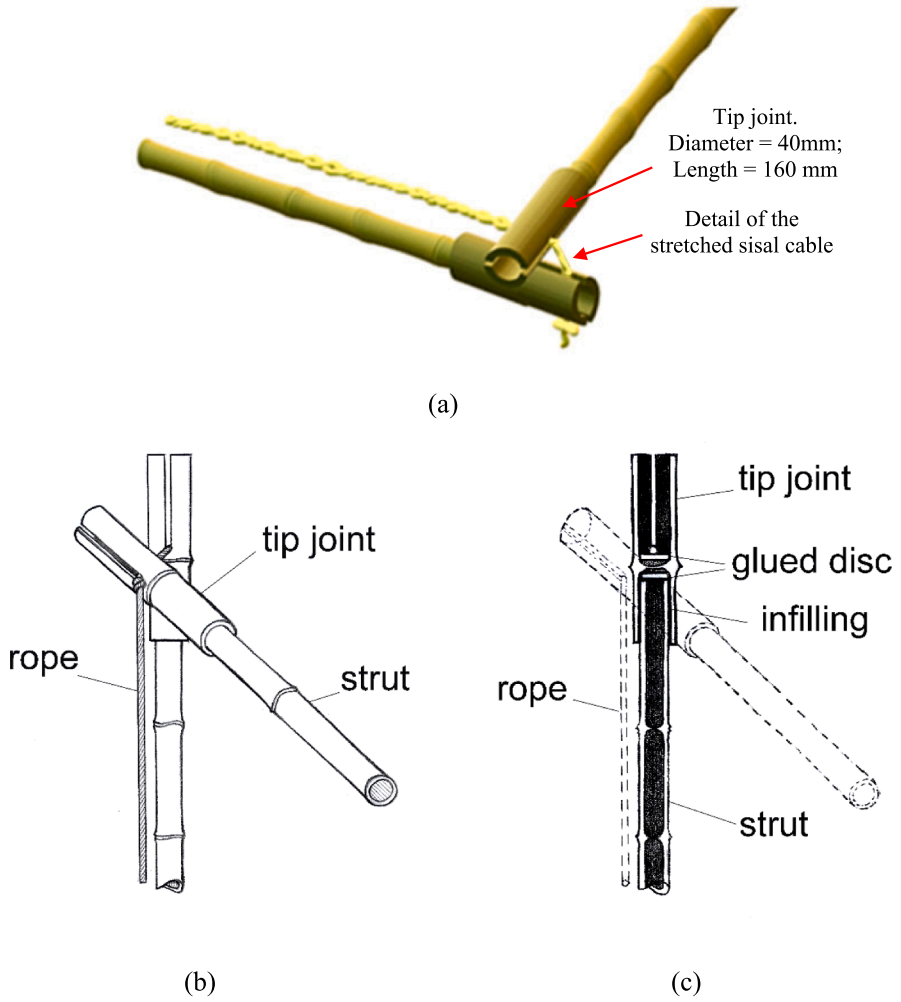

Fig. 3. Bamboo strut-cord reciprocal connection developed at the Laboratory of Investigation in Living Design (LILD/PUC-Rio) and designed for a bamboo-sisal rope system: (a) 3D view; (b) detail of the strut-cord connection; (c) front view of the joint in section.

cables. The influence of time-dependent material properties to the behavior is also investigated.

As detailed in the previous paragraph, the scope of the work is limited to the self-stress state of a single module. It is a relevant stage of the tensegrity behavior, responsible for the structural stability, and has been also the focus of previous works [29–31]. Therefore, this work intends to present the system's feasibility, providing insights and opening the possibility to future developments on the field. It is noteworthy that the effects of external loads and the influence of overall span should be considered in the structural design and ultimate and serviceability limit states must be appropriately checked. The ultimate limit states for a self-supporting bamboo structure with flexible joints were investigated by Seixas et al. [28] showing a stable and symmetrical behavior under static loadings until collapse, indicating that bamboo poles can be used as a suitable material for this use.

2. Module description and constructional aspects

2.1. Module description

The structural geometry selected for this work is inspired on the pentagonal "hollow-rope" tensegrity pedestrian bridge proposed by Rhode-Barbarigos et al. [15], also adopted in other studies [32]. The main motivation behind the use of this model herein relies on its feasibility as an engineering solution for application in large-scale construction, as it can meet safety and serviceability criteria according to structural design standards [15,17]. Furthermore, it was shown that a pentagonal tensegrity ring module is the most efficient configuration when compared to squared and hexagonal modules in terms of an efficiency index that takes into account the self-weight, serviceability performance and overall stiffness of the structure [15]. Concurrently, the tensegrity ring module topology allows cable-length changes during folding and unfolding of the structure [16], encouraging the fully handcrafted deployment of the bio-based tensegrity module proposed in this study (see Section 2.2).

The original geometry was designed with four 5 m length individual tensegrity modules interconnected to overcome a total span of 20 m, as shown in Fig. 1a. The modules are based on a pentagonal prism containing fifteen nodes to outline three pentagonal layers. Fifteen struts are compressed by thirty cables connected on the ends of the struts to form a modular tensegrity unit. Struts can be separated into two categories: (i) main struts and (ii) scissor struts. The first group depicts the five compressive members which bind the two outer pentagons, while the second group portrays the ten elements linking the middle pentagon to the external ones. Likewise, the cables are classified based on their position: (i) ten layer cables (L-cables) form the two outlying pentagons and (ii) twenty X-cables link scissor struts nodes to outer pentagon nodes, as seen in Fig. 1b. Each individual module has a length of 500 cm in which main and scissor struts are 678 cm long, layer cables have 458 cm and x-cables have 347 cm, that ensures an adequate free space for pedestrian circulation (Fig. 1c). The tables of nodal coordinates and members' connectivity for a single full-scale module are presented in

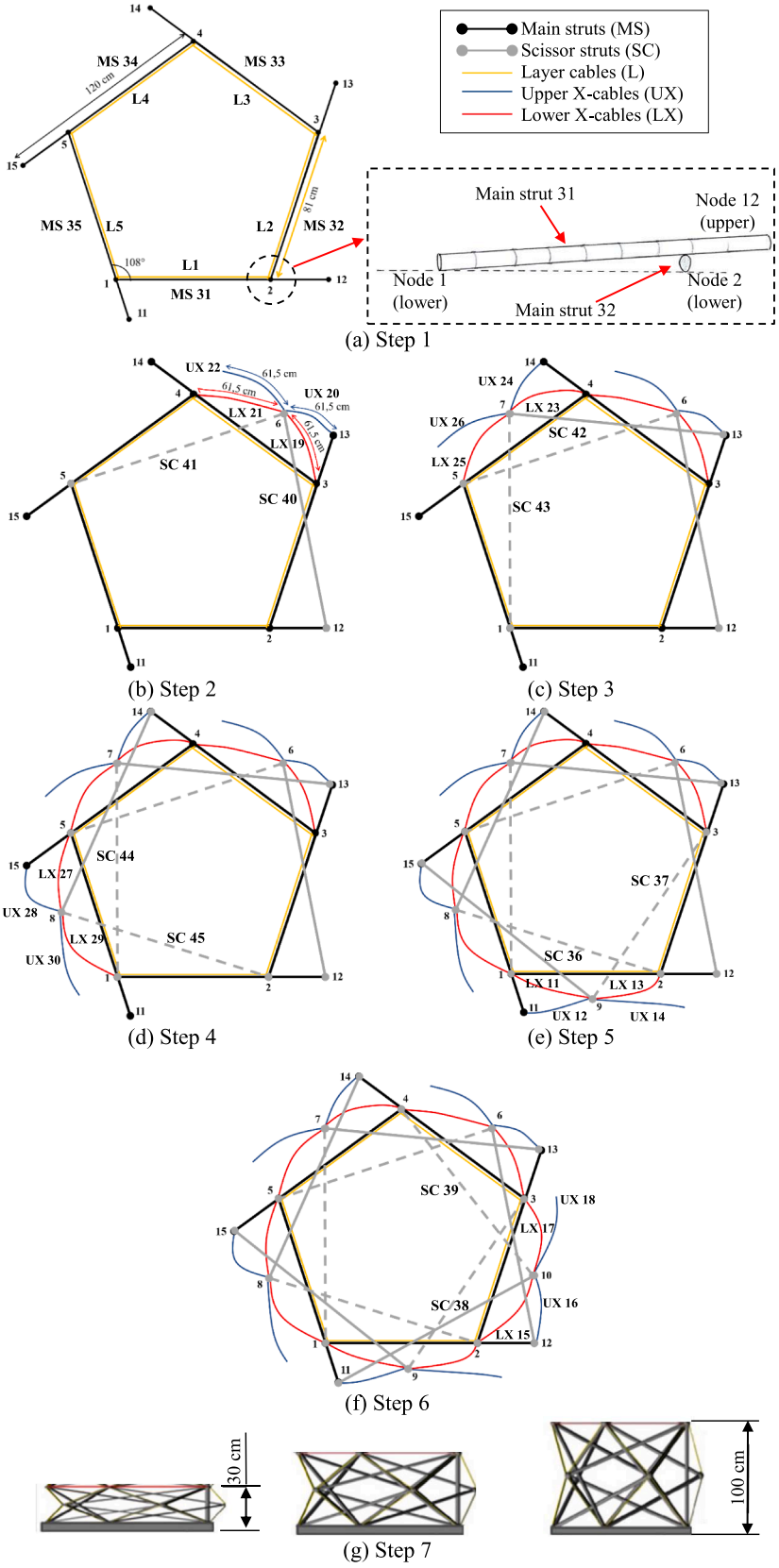

Fig. 4. Module assembly sequence: (a) step 1 to (f) step 6 corresponds to the plan view of the procedure and (g) step 7 corresponds to the side view of the procedure (elevation view).

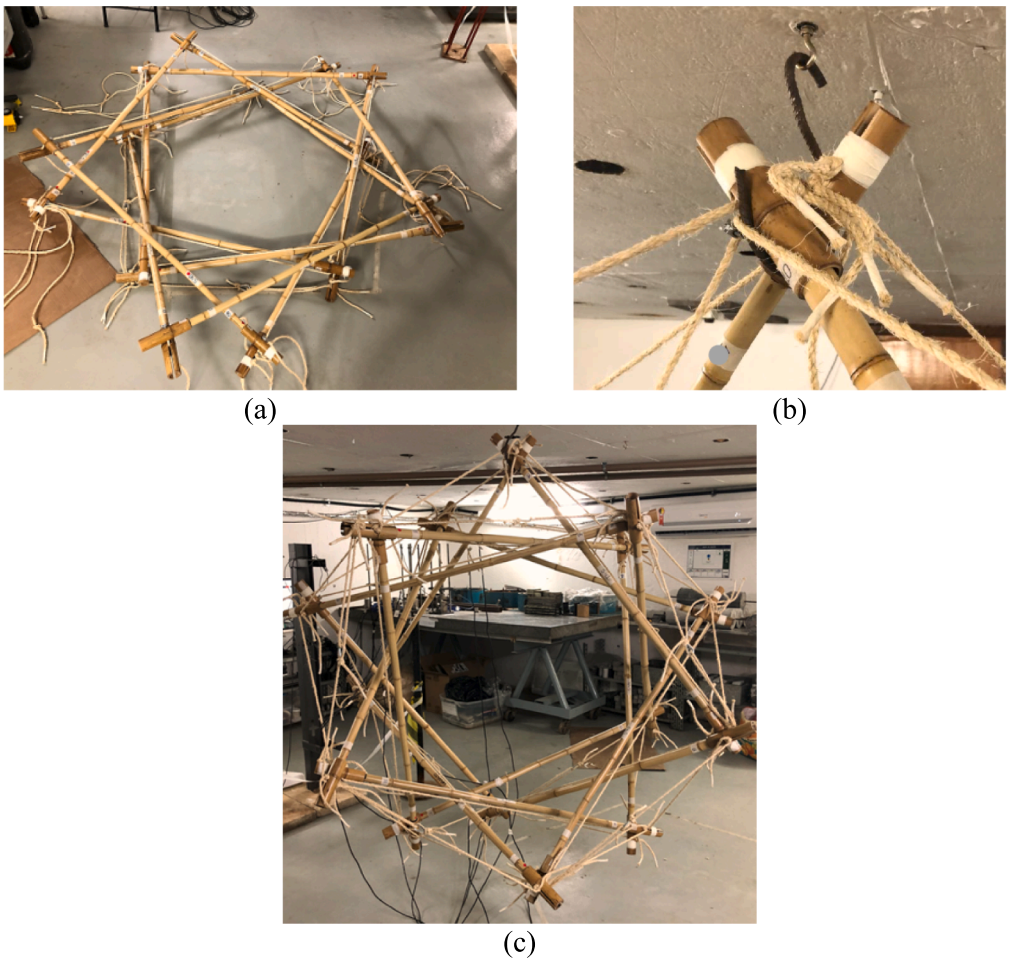

Fig. 5. Model in 1:5.65 scale: (a) module on the ground before expansion; (b) detail of hook for suspension of the module; (c) module after deployment.

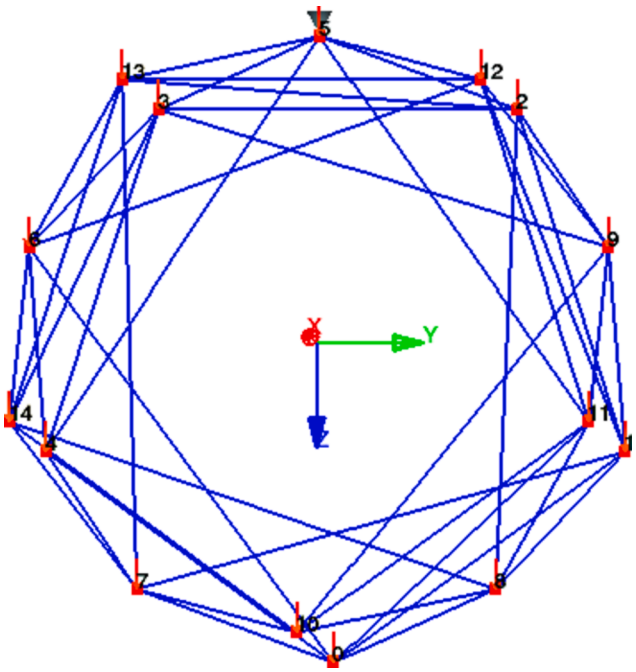

Fig. 6. Frontal view (Y-Z plane) of the computational model for the analysis of the tensegrity module using Galileo program [40].

Table 1 and Table 2, respectively. In the present study, however, the reduced scale physical model was built in a scale of 1:5.65, with 120 cm long struts and layer cables and X-cables having respectively 81 cm and 61.5 cm in length.

The tensegrity bridge proposed by Rhode-Barbarigos et al. [15] is made entirely of steel. In the present work, to obtain a bio-based tensegrity structure, full-culm bamboo was adopted for the struts whereas sisal (*Agave sisalana*) ropes were adopted for the cables. *Phyllostachys aurea* bamboo species was selected due to its physical and mechanical properties, workability and commercial availability in Brazil [28]. In turn, sisal is a vegetable material from the Latin-American biodiversity and the sisal rope is a traditional artifact locally produced in the Brazilian Northeast region that remains unexplored in bio-based engineering structures due to the lack of technical information, despite its large application in craftsmanship. Due to their great potential for sustainability, both materials were selected for the design of a fully reversible tensegrity structure [33,34]. Table 3 presents the cross-sectional dimensions of bamboo members and sisal ropes, as well as their relevant average mechanical properties, obtained from specific tests according to ISO 22157-1:2004 [35] (currently ISO 22157-1:2019 [36]) and TDC8 (5628)P3 [37], respectively. It is important to highlight that the structure was initially designed for a low prestress level of 5% with respect to the tensile strength of the sisal cables [15].

2.2. Constructional aspects

Before constructing the module in the aforementioned desired scale, a 1:25 small scale physical model was constructed using bamboo sticks

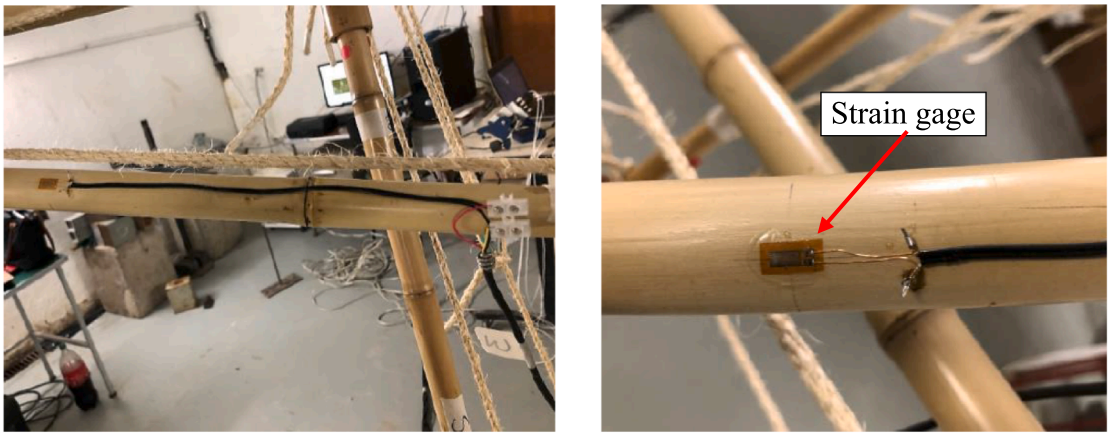

Fig. 7. Strain gages installed to measure strains during static test (a) and (b) detail view.

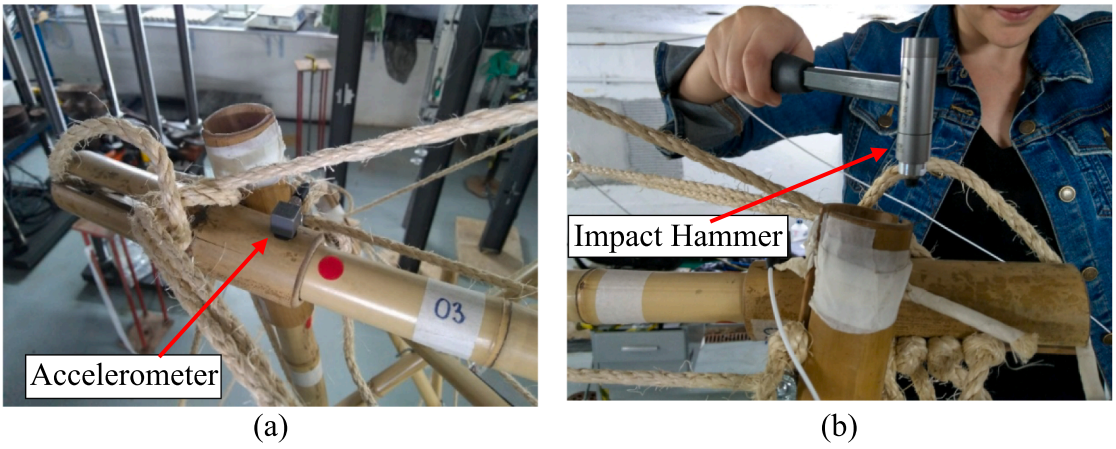

Fig. 8. Instrumentation and execution of the dynamic testing: (a) location of the accelerometer on the joint; (b) application of impact with an instrumented hammer.

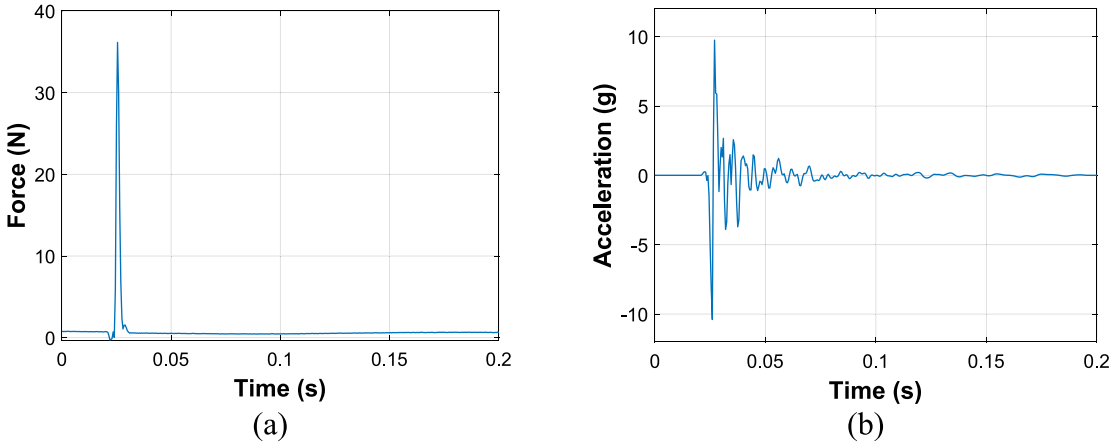

Fig. 9. Experimental dynamic signals in time domain at the driving point, i.e. where the impact and the response occur at the same location (main strut 33): (a) impulse force of the instrumented hammer; (b) acceleration response.

and synthetic strings, as shown in Fig. 2. The construction methodology was developed to allow the module to be fabricated and deployed using readily available tools. Therefore, the 1:25 scale model contributed to anticipate challenges beforehand – details about this model are given in Albuquerque [38].

Based on this preliminary study, it was decided to adopt an adaptation of the Tensegritoy modeling kit, where each wooden rod working as a strut has a notch at both ends to which the rubber band strings are attached; aluminum caps are used to lock these ends afterwards [39]. In this model, the notch was made at both ends of the bamboo stick. The string is attached to the stick by means of a knot at each end that prevents the string from slipping through the notch.

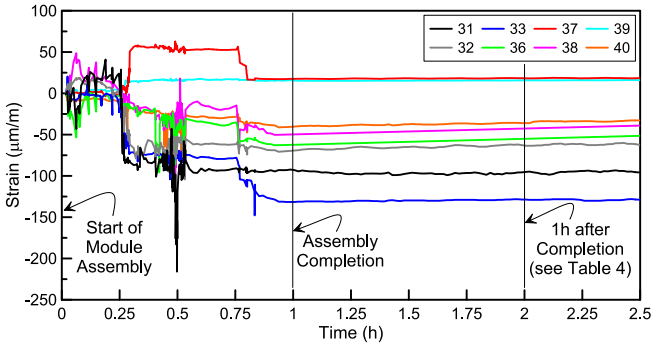

Fig. 10. Evolution of strains over time captured in the main struts (MS) 31, 32, 33, and scissors (SC) 36, 37, 38, 39, 40.

Therefore, this adaptation focuses on the development of a fully bio-based tensegrity structure without the utilization of metallic elements, also considering the end-of-life biodegradability of the structure in the design of joints. Thus, proper tip joints for tensegrity bamboo structures developed at the Laboratory of Investigation in Living Design (LILD) from PUC-Rio were applied for the physical scale models, as seen in Figs. 3 and 4 [10]. For the 1:5.65 model, bamboo strut-cord reciprocal joints with a diameter of approximately 40 mm and 160 mm long were used (Fig. 3a). In each tip joint, 90 mm deep × 7 mm wide notches were introduced to allow for the attachment of 6 mm sisal ropes (Fig. 3b). Bamboo culms were rigorously selected, allowing for a good coupling between struts and joints. Infillings using fabrics were crafted for a better transmission of forces in the strut-cord joint, ensuring tightness. Bamboo discs with minor diameters were glued into the cavities of the joints for transferring of the cable forces to the diaphragm in the middle of the joint, as observed in Fig. 3c.

The assembly of the module is divided into seven main steps, as depicted in Fig. 4. The first one relates to the layout of the main struts (MS 31 to MS 35 – black lines) which form a pentagon on the ground (see Fig. 4a). It should be noted that the nodes from numbers 1 to 5 are at a lower position compared to those from numbers 11 to 15 (upper nodes). The reader is referred to check also Table 2 regarding the connectivity of members. Afterwards, the first five layer cables (L1 to L5 – yellow lines) bind the closed path among the lower nodes of the regular polygon.

The subsequent steps from two to six present the mounting of the scissor struts (SC 36 to SC 45 – gray lines) and X-cables (11 to 30) on the main struts. For an easy understanding of the assembly method, the X-cables were divided into two subgroups: upper (even- numbered UX – blue lines) and lower (odd-numbered LX – red lines). Thus, as exhibited in Fig. 4b (step 2), the SC 40 and 41 members are located between the nodes 3 and 4 of the MS 33 and share a common joint (node 6). In turn, they are also connected to the nodes 12 and 5 of the MS 31 and 34, respectively. It is worth noting that the solid gray lines refer to scissor struts crossing over the main struts, while the dashed ones to the crossing beneath them. Subsequently, the X-cables are ready to be connected to the adjacent upper and lower nodes of the pentagon, apart from the UX 14, 18, 22, 26 and 30, which will be tied later in the seventh step.

This way, the same procedure is repeated four more times, following Fig. 4c, d, e and f. At the end of step 6, all elements of the module are connected, except for the UX cables mentioned beforehand and the remaining five layer cables (L6 to L10). By means of temporary cables attached to the nodes 11 to 15, the structure should be suspended using a mast or by a volunteer. Fig. 4g shows a schematic of the module deployment. Finally, the last UX and layer cables are linked to the lower and upper nodes of the main struts, respectively. Thereafter, the tensegrity structure is active and ready for use as seen in Fig. 5.

Table 4
Experimental strains and computed stresses over time. The negative sign indicates compressive strains, while the positive sign indicates tensile strains.

Strut	t = 2 h		t = 324 h	
	Experimental strain (με)	Experimental Stress (MPa)	Experimental strain (με)	Experimental Stress (MPa)
31 (main)	−93.20	−1.81	93.38	1.81
32 (main)	−63.49	−1.23	−119.66	−2.32
33 (main)	−129.00	−2.51	−147.11	−2.86
36 (scissor)	−46.33	−0.90	−54.53	−1.06
37 (scissor)	19.30	0.37	18.90	0.36
38 (scissor)	−34.54	−0.67	−32.20	−0.63
39 (scissor)	16.11	0.31	15.49	0.30
40 (scissor)	−30.70	−0.60	−107.00	−2.09

Table 5
Normal stresses in the struts for different percentages of prestress (S_0).

Level of prestress, S_0 (%)	Normal stresses (MPa)							
	Main struts (MS)			Scissor struts (SC)				
	31, 35	32, 34	33	36, 45	37, 44	38, 43	39, 42	40, 41
0.25	−0.11	−0.03	−0.25	−0.03	−0.02	+0.02	−0.06	+0.03
2.50	−0.33	−0.21	−0.39	−0.11	−0.09	−0.06	−0.11	−0.02
5.00	−0.62	−0.50	−0.67	−0.22	−0.19	−0.17	−0.21	−0.13
10.00	−1.19	−1.09	−1.24	−0.43	−0.40	−0.38	−0.42	−0.34
15.00	−1.75	−1.66	−1.80	−0.65	−0.62	−0.60	−0.64	−0.56
20.00	−2.32	−2.24	−2.36	−0.87	−0.85	−0.82	−0.87	−0.78
25.00	−2.89	−2.81	−2.93	−1.11	−1.08	−1.06	−1.10	−1.02
30.00	−3.46	−3.38	−3.49	−1.35	−1.32	−1.30	−1.34	−1.26
35.00	−4.02	−3.95	−4.05	−1.59	−1.57	−1.55	−1.59	−1.51
40.00	−4.58	−4.52	−4.61	−1.84	−1.82	−1.80	−1.84	−1.76
45.00	−5.15	−5.08	−5.17	−2.10	−2.08	−2.05	−2.09	−2.02
50.00	−5.70	−5.65	−5.73	−2.36	−2.34	−2.31	−2.35	−2.28

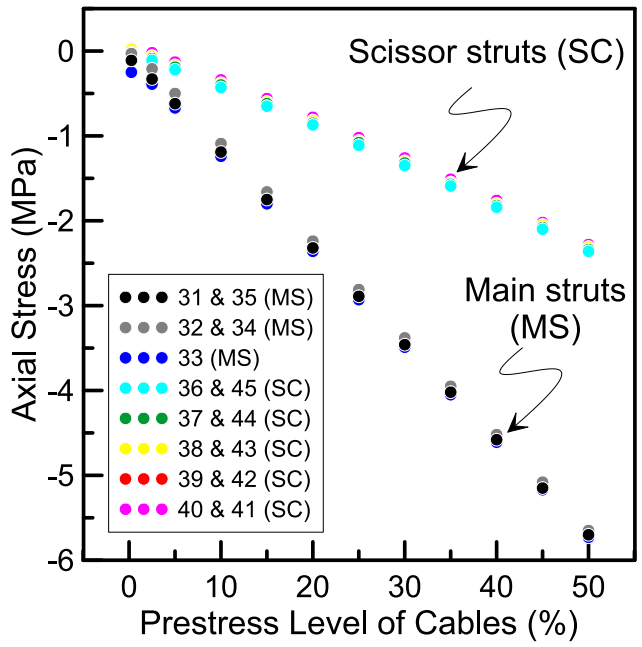

Fig. 11. Variation of the numerical axial stress of the module with the prestress level of cables regarding its main struts (31 &35, 32 & 34 and 34) and scissor struts (36 &45, 37 & 44, 38 & 43, 39 & 42 and 40 & 41.

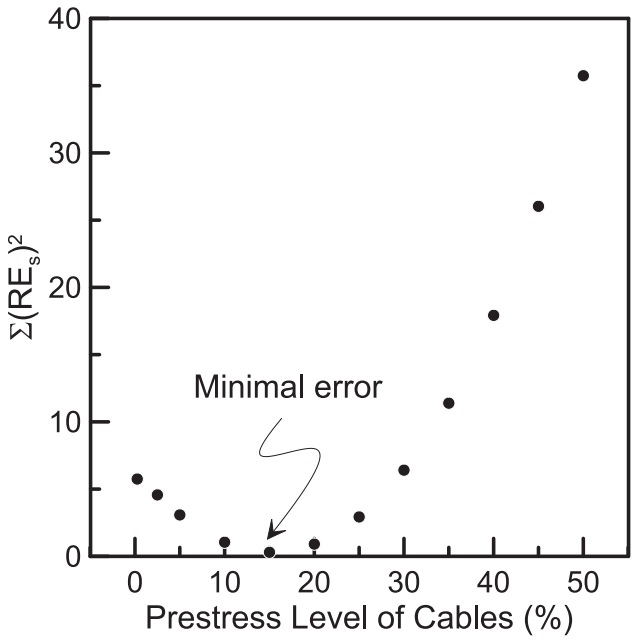

Fig. 12. Sum of squares of the static relative error, $\Sigma(RE_s)^2$, for prestress level of cables varying from 0.25% to 50% and identification of the minimal error at 15%.

Table 6
Static relative errors (RE_s) for instrumented struts (31, 32, 33, 36, 38 and 40) and sum of squares for different levels of prestress varying from 0.25% to 50%.

Prestress Level, S_0 (%)	RE_s						$\Sigma(RE_s)^2$
	31	32	33	36	38	40	
50	2.15	3.59	1.28	1.62	2.45	2.82	35.74
45	1.84	3.13	1.06	1.33	2.06	2.38	26.03
40	1.53	2.67	0.84	1.05	1.68	1.95	17.92
35	1.22	2.21	0.61	0.77	1.30	1.53	11.39
30	0.91	1.75	0.39	0.50	0.94	1.11	6.41
25	0.60	1.29	0.17	0.23	0.58	0.71	2.93
20	0.28	0.82	−0.06	−0.03	0.23	0.32	0.91
15	−0.03	0.35	−0.28	−0.28	−0.11	−0.06	0.30
10	−0.34	−0.12	−0.51	−0.53	−0.44	−0.43	1.05
5	−0.66	−0.59	−0.73	−0.76	−0.75	−0.79	3.08
2.5	−0.82	−0.83	−0.84	−0.87	−0.91	−0.96	4.57
0.25	−0.94	−0.98	−0.90	−0.97	−1.03	−1.05	5.75

3. Numerical simulation and experimental program

3.1. Numerical model

As shown previously, the fabrication and assembly of the proposed bio-based tensegrity module did not require any special tool and there is no specific device to control initial prestress. The level of prestress applied to the sisal ropes is determined indirectly by computing the relative errors between the numerical and experimental results leading to a minimum error, as can be visualized later in Section 4. For that, a numerical model using the Galileo software [40] – developed for static and dynamic structural analysis of deployable structures and tensegrities – was used. The prestress level is introduced in the computational model as an input from which the current stress level at each material point of each element can be computed via a constitutive law. In practice, the prestress level can be obtained from a deviation on each element's length due to fabrication errors or thermal variations. A significant length error value on the obtained range is chosen and is converted to stresses via the material's constitutive law. The following hypotheses are considered: a) cables and struts are straight and are connected through nodes; b) members are elastic and perfectly articulated (moment-free) at the nodes; c) struts can carry either tensile or compressive forces whereas cables can only carry tensile forces; d) initial geometry and prestress conditions are previously established; e) the prestress level is the same for every cable; f) local and global buckling of struts are neglected; g) increments in stiffness that may be caused by external loads are disregarded; h) the module is subjected only to gravity load applied to the nodes; and i) materials behavior is assumed to be linear elastic. Cross-section dimensions and materials properties considered in the model follow those reported in Table 3. For the boundary conditions, it was assumed that the module was suspended at node 6, i.e. preventing translations in all directions. An overview of the numerical model is presented in Fig. 6. It is important to mention that bamboo, as a natural material, is naturally curved. In the aforementioned model, members are considered straight, although formulations for geometrically non-linear analysis of curved members are also available [41,42].

3.2. Static testing

The primary objective of performing the static test was to experimentally evaluate the stresses acting on the struts during and after erection. To accomplish this task, the physical model was instrumented with eight 120 Ω strain gages in order to measure the specific strains for each stage. The electrical signals from the strain gages were conditioned by the NI 9235 module (¼ bridge) connected to the cDAQ-9174 chassis, both from National Instruments. The following struts were selected to be instrumented with a single gage: MS 31, MS 32, MS 33, SC 36, SC 37, SC 38, SC 39 and SC 40. Apart from MS 33, these struts presented symmetrical axial force pairs (31;35), (32;34), (36;45), (37;44), (38;43), (39;42) and (40;41) based on a static analysis using Galileo program [40], as will be discussed in Section 4.1. Although members of tensegrity structures are assumed to be subjected to pure axial force, other internal forces may arise due to imperfections associated to eccentricity at the connections and out-of-straightness of members [43]. Therefore, one of the main difficulties lies in the fact that the reading of the gages may be influenced by bending moments. Fig. 7 shows the strain gage installed in

Table 7
Natural frequencies (Hz) of the first ten vibration modes depending on the percentage of prestress (S_0) varying from 0.25% to 30%.

S_0 (%)	Natural frequencies (Hz)									
	M1	M2	M3	M4	M5	M6	M7	M8	M9	M10
0.25	0.67	0.70	1.23	9.08	13.13	16.14	16.77	30.58	30.94	43.50
2.5	2.12	2.20	3.89	9.59	14.12	16.95	17.75	30.87	31.35	43.74
5.0	2.98	3.10	5.50	10.10	15.14	17.80	18.77	31.18	31.79	44.00
7.5	3.63	3.78	6.74	10.57	16.10	18.62	19.75	31.50	32.24	44.26
10.0	4.18	4.35	7.78	10.99	16.99	19.40	20.68	31.82	32.68	44.52
12.5	4.65	4.84	8.70	11.39	17.83	20.16	21.58	32.13	33.12	44.78
15.0	5.08	5.28	9.53	11.76	18.63	20.88	22.44	32.45	33.56	45.04
17.5	5.46	5.69	10.29	12.11	19.38	21.59	23.27	32.76	33.99	45.30
20.0	5.82	6.06	11.00	12.44	20.10	22.27	24.07	33.08	34.42	45.56
22.5	6.15	6.41	11.66	12.75	20.79	22.93	24.84	33.39	34.85	45.82
25.0	6.46	6.74	12.29	13.04	21.45	23.58	25.60	33.71	35.28	46.07
27.5	6.75	7.05	12.88	13.33	22.09	24.21	26.33	34.02	35.70	46.33
30.0	7.03	7.34	13.42	13.63	22.70	24.82	27.04	34.34	36.12	46.58

Table 8
42 Natural frequencies (Hz) and percentage change of the module for the extreme values of prestress levels (0.25% and 30%).

Mode	Prestress level		Percentage change (%)	Mode	Prestress level		Percentage change (%)
	0.25%	30.00%			0.25%	30.00%	
1	0.67	7.03	942.0%	22	125.30	127.39	1.7%
2	0.70	7.34	951.8%	23	137.82	139.85	1.5%
3	1.23	13.42	990.6%	24	138.83	140.83	1.4%
4	9.08	13.63	50.0%	25	143.09	145.37	1.6%
5	13.13	22.70	72.9%	26	146.53	148.72	1.5%
6	16.14	24.82	53.7%	27	149.06	151.63	1.7%
7	16.77	27.04	61.2%	28	200.45	201.43	0.5%
8	30.58	34.34	12.3%	29	207.79	208.96	0.6%
9	30.94	36.12	16.7%	30	245.89	246.55	0.3%
10	43.50	46.58	7.1%	31	260.65	261.42	0.3%
11	46.08	49.30	7.0%	32	274.25	274.97	0.3%
12	53.52	56.78	6.1%	33	306.46	307.43	0.3%
13	67.14	69.82	4.0%	34	310.27	311.15	0.3%
14	70.42	73.10	3.8%	35	323.99	324.39	0.1%
15	76.49	78.76	3.0%	36	331.90	332.99	0.3%
16	77.97	80.37	3.1%	37	342.01	343.03	0.3%
17	83.26	85.96	3.2%	38	350.17	351.18	0.3%
18	83.99	86.58	3.1%	39	356.92	357.99	0.3%
19	95.50	97.68	2.3%	40	370.96	371.94	0.3%
20	99.65	102.05	2.4%	41	375.83	376.83	0.3%
21	111.63	114.22	2.3%	42	378.46	379.46	0.3%

one of the struts. The assembly of the module took approximately 1 h and the strains were captured for a total period of 324 h (13.5 days) including the assembly procedure, therefore allowing monitoring the loss of prestress during the early days after the assembly due to the time-dependent phenomena that may affect importantly the performance of mechanical natural materials. During the test, the module was kept in a room with controlled temperature and humidity (22.8 °C ± 0.4 °C and 49.6% ± 2.0%, respectively).

3.3. Dynamic testing

The dynamic testing was carried out to determine the natural frequencies of the tensegrity module. Therefore, the influence of ageing on the prestress level was indirectly investigated through the variation of the natural frequencies considering four dynamic experimental tests: the first one immediately after the assembly of the module, the second one after 4 days, the third one after 14 days and, finally, the last test was performed 52 days after the conclusion of the assembly. The temperature and humidity of the room during this period were equal to 23.3 °C ± 0.7 °C and 47.6% ± 2.7%, respectively.

A well-established experimental modal analysis was performed using the single-input/single-output (SISO) technique [44,45] by means of an impact hammer – input signal – and a piezoelectric accelerometer – output signal (types PCB Piezotronics 086C03 and 333B40, respectively) as shown in Fig. 8. The signals were acquired through the cDAQ-9174 acquisition system from National Instruments (NI), equipped with Integrated Electronic Piezoelectric (IEPE) analogue input modules (NI 9233) with a sampling frequency of 2000 Hz. The tests were performed and processed using ARTeMIS program [46]. The piezoelectric accelerometer was fixed on the strut 33, over node number 03, to measure the free vibration of the module in terms of acceleration in the vertical direction. In turn, the structure was excited vertically by an impulsive load over all nodes of the structure, apart from the support node number 06. The measurement time of each impact test per node was set equal to 4.096 s, which was enough for the total dissipation of the dynamic response to occur, as depicted by Fig. 9. Furthermore, for every test, a total of 10 impacts per node was carried out for signal averaging purposes in frequency domain [44].

4. Results

4.1. Static analysis

The evolution of experimental strains for the struts instrumented within the first 2.5 h is presented in Fig. 10. It can be seen that the strains oscillated considerably during the construction phase and finally stabilized after the first hour, when the module assembly was completed. It must be highlighted that some of the readings indicated tension (struts

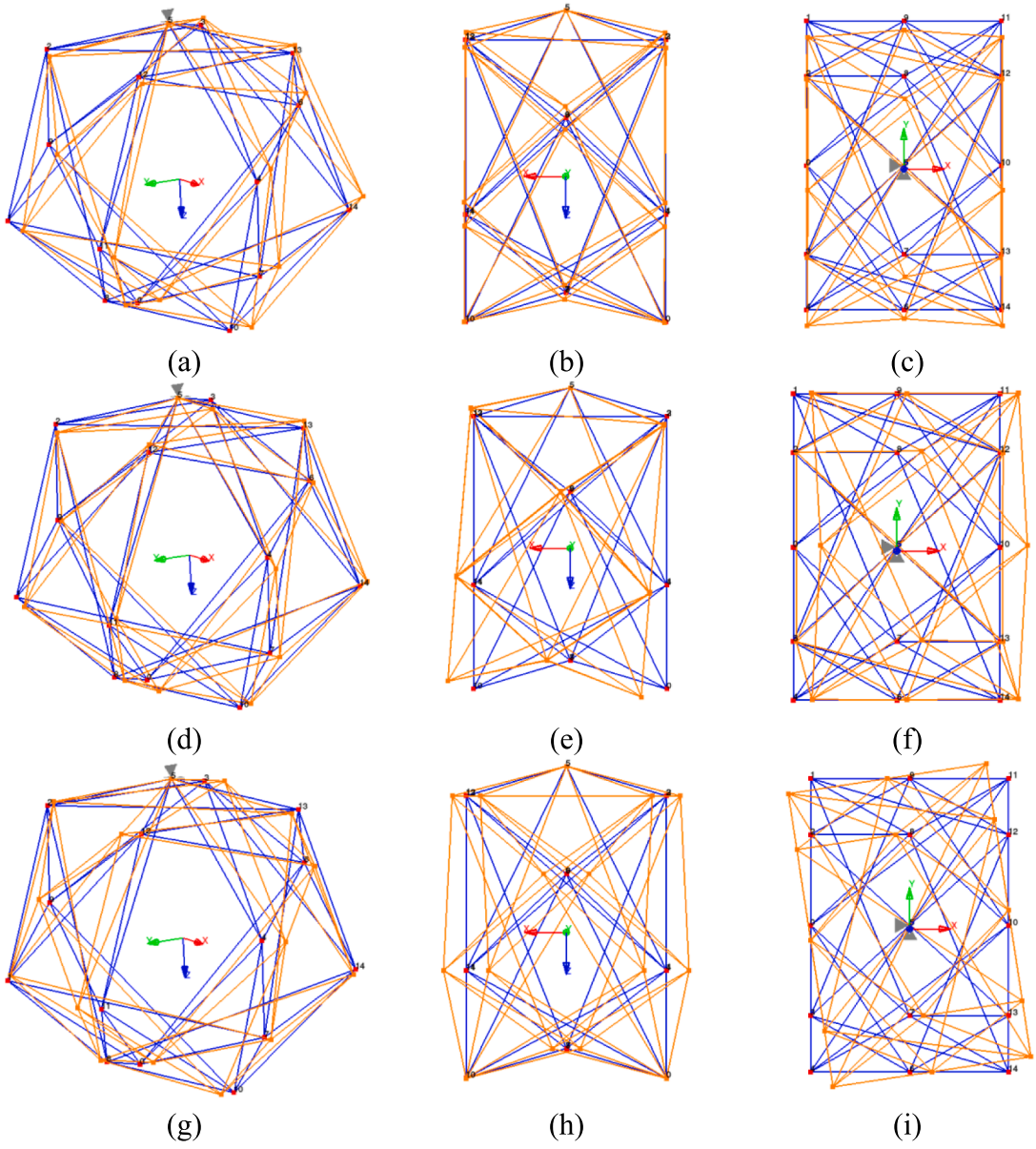

Fig. 13. Vibration modes obtained from the numerical model (Galileo program [40]) considering a prestress level of 5%: isometric, lateral (X-Z plane) and upper (X-Y plane) view of the first lateral mode (a, b and c) in the Y direction (f = 2.98 Hz); the second lateral (d, e and f) in the X direction (f = 3.10 Hz) and the first torsional (g, h and i) about the vertical Z-axis (f = 5.50 Hz), respectively. The blue lines indicate the undeformed model whereas the orange ones correspond to the deformed shapes. (For interpretation of the references to colour in this figure legend, the reader is referred to the web version of this article.)

37 and 39), which may be associated to bending induced by system imperfections mentioned in Section 3, as well as to bending caused by distributed dead weight. Table 4 summarizes the strains 1 h after the assembly completion (t = 2 h) and after 324 h of test. The equivalent stresses, also reported in the Table 4, were computed multiplying the strains by the bamboo modulus of elasticity of 19.4 GPa (see also Table 3).

From Table 4, it can be seen a strain increase of 88%, 14%, 18% and 249% for MS 32, MS 33, SC 36 and SC 40, respectively, indicating greater compressive stresses, especially in the former and latter elements, while SC 38 exhibited a slight stress relief (reduction) of 7%. In turn, SC 37 and SC 39 also presented a modest strain decrease of 2% and 4%, respectively, depicting lower tensile stresses. Interestingly, it can be noticed that MS 31 behaved conversely over time, i.e., varying from compressive (t = 2 h) to tensile (t = 324 h) strains equal to −93.20 με and 93.38 με, respectively. One reason for this may be a compensating effect of the inequality in the acting forces in order to keep the whole system in equilibrium, which may also produce a variation in the strut stresses that are not monitored. Another possible explanation concerns to the creep effect of bamboo, since this material shows creep behavior not only after a long period of time, but also after a short interval after loading, due to the ease deformation of the lignin (organic molecule associated with stiffness) within the bamboo microstructure [47,48]. This phenomenon should be further investigated.

Regarding the numerical static analysis performed with Galileo software, the influence of the prestress levels (S_0) on the normal stresses of the module was investigated, ranging from 0.25% to 50%. As expected, the prestress level had a direct impact on the compressive stresses of the struts, as shown in Table 5 and Fig. 11. It can be noted that as higher the level of prestress is, as greater the compression stress (negative values) is observed, presenting a nearly linear behavior for both main and scissor struts. For values of S_0 below 2.5%, some struts experienced tensile stresses (positive values). In general, the compression stresses of the main struts were three times higher from those

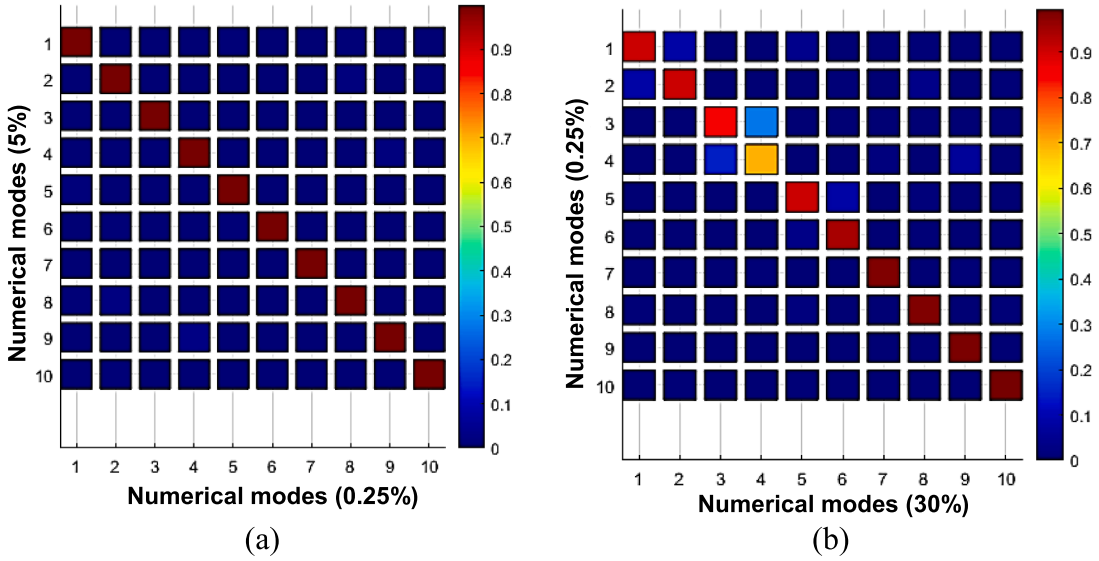

Fig. 14. Modal Assurance Criteria (MAC) matrix among the first ten numerical mode shapes: (a) prestress level of 0.25% and 5%; (b) prestress level of 0.25% and 30%. Values close to the unity (1) indicate a high correlation between the two modal vectors.

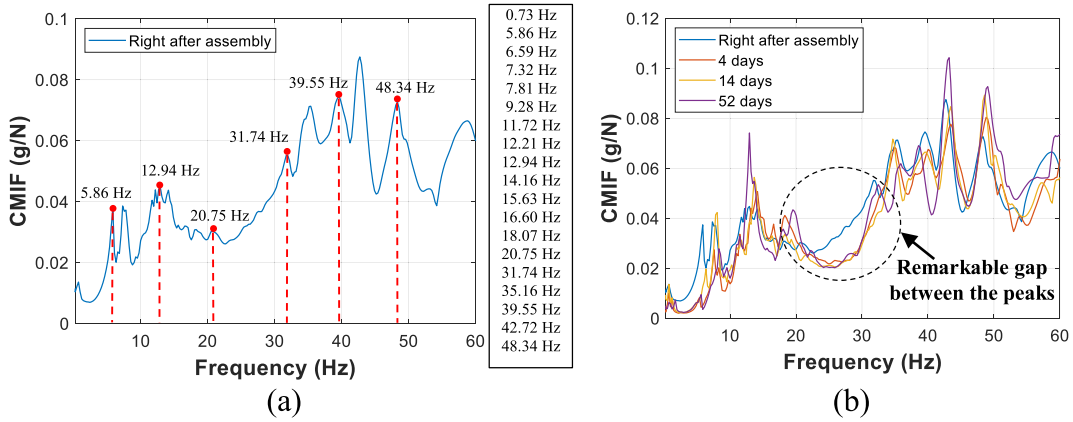

Fig. 15. Complex Mode Indicator Function (CMIF) of the tensegrity module concerning the experimental dynamic testing: (a) right after assembly (some of the noticeable peaks are indicated by red dots with a complementary full list to the right); (b) right after assembly (blue line), 4 days after (red line), 14 days after (yellow line) and 52 days after (magenta line). (For interpretation of the references to colour in this figure legend, the reader is referred to the web version of this article.)

experienced by scissor struts.

Therefore, to determine indirectly the level of prestress of the module, a comparison between numerical and experimental compressive stresses – σ_{num} and σ_{exp}, respectively – was made by means of a relative error parameter, RE_s, calculated for each individual strut as follows:

$$RE_s = \frac{\sigma_{num}(S_0) - \sigma_{exp}}{\sigma_{exp}} \quad (1)$$

Notice that the subscript "s" denotes static analysis. This way, Table 6 presents the relative errors obtained for the struts analyzed for different levels of prestress considering σ_{exp} for t = 2 h (1 h after the assembly completion). It is worth noting that, because SC 37 and SC 39 presented experimental tensile stresses, they are not suitable for comparison with the results from the computational model and therefore were not considered in Eq. (1). As an example, it can be noted that, for MS 31, the minimum error was achieved near 15% of prestress. In general, for an individual comparison, it can be seen that that the minimum relative error is around 10% to 25% of prestress. To take into account the full set of struts instrumented, the sum of the squares of the relative errors were computed, as also presented in Table 6. It is finally possible to observe that there is a minimum error value associated with the overall behavior of the tensegrity module closest to 15% of prestress, as shown in Fig. 12. It should be mentioned that the static numerical analysis performed does not consider the creep effect over time. Thus, the REs for 324 h of test is beyond the scope of this work. Nevertheless, as mentioned previously in Section 3.3, the influence of ageing on the prestress level of cables is investigated based on an experimental dynamic analysis as presented in Section 4.2.

4.2. Dynamic analysis

The computational model developed in the Galileo software [40] for the undamped free vibration analysis takes into consideration the mass matrix and the nonlinear stiffness matrix of the module. Through the modal analysis performed by the software, 42 axial vibration modes were obtained. It is worth noting that in case of evaluating the dynamic behavior of compressed members near buckling, which is beyond the scope of this paper, it is appropriate to consider the coupling between transversal and axial stiffness of each component using non-linear Euler–Bernoulli beam elements [23,25], allowing the representation of bending-type modes.

Table 7 shows the natural frequencies of the tensegrity module

Table 9
Noticeable peaks related to the natural frequencies from the Complex Mode Indicator Function (CMIF) of the tensegrity module right after the assembly and 4, 14 and 52 days after its conclusion.

Number of noticeable peaks	Natural frequencies (Hz)			
	Right after assembly	4 days	14 days	52 days
1	0.73	0.73	0.73	0.73
2	–	1.22	1.22	1.71
3	5.86	5.37	–	5.62
4	6.59	–	6.35	–
5	7.32	7.57	–	–
6	7.81	8.30	8.06	8.30
7	9.28	9.77	9.23	9.52
8	–	–	10.25	–
9	–	10.99	10.99	–
10	11.72	11.47	11.72	11.47
11	12.21	–	–	–
12	12.94	–	12.94	12.94
13	–	13.18	13.67	13.67
14	14.16	14.16	–	–
15	15.63	–	–	–
16	16.60	16.60	16.36	–
17	18.07	18.31	18.31	18.07
18	–	–	19.29	19.53
19	20.75	–	21.48	22.22
20	31.74	–	–	32.47
21	35.16	34.91	34.67	35.89
22	–	38.09	37.11	38.57
23	39.55	40.04	39.55	–
24	42.72	43.46	43.46	43.21
25	48.34	48.83	48.58	49.07

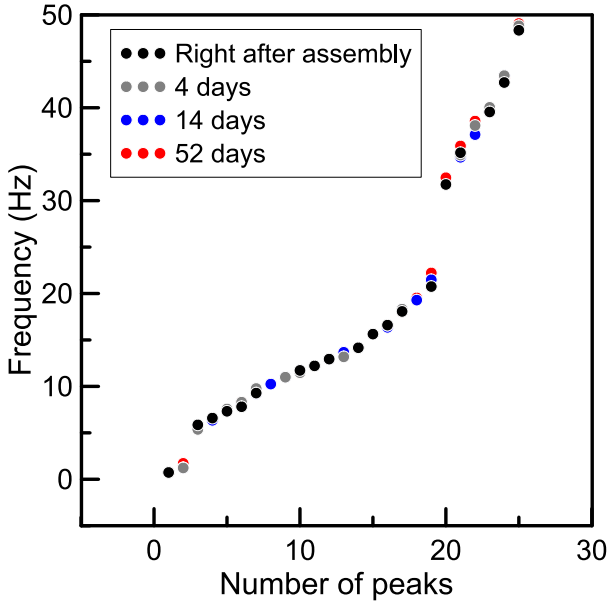

Fig. 16. Experimental natural frequencies of the tensegrity module considering its first twenty-five peaks right after assembly and after 4, 14 and 52 days.

related to the first ten modes of vibration, varying from 0.67 Hz to 46.58 Hz, considering different prestress levels. It is noticed that the frequencies increase not only according to the succession of modes of vibration for the same level of prestress, but also considering only a single mode and different levels of prestress (S_0). Although there are 42 vibration modes, it was seen that after the 9th mode the percentage variation of the natural frequency as a function of the increase of the prestress level is less than 10% when the extreme values of the prestress levels (0.25% and 30%) are compared, as displayed in Table 8. Such behavior indicates that these first vibration modes are more influenced by the prestress level applied to the structure. Thus, the vibration modes above the 10th mode were disregarded henceforth in this analysis.

Because tensegrity module is a complex three-dimensional structure, the visualization of their vibration modes is not a simple task, as shown in Fig. 13, which depicts the first three vibration modes for a prestress level of 5%. Thus, the behavior of the mode shapes are better evaluated through the well-known Modal Assurance Criterion (MAC) [45,46,49], as defined by Eq. (2), where $\{\psi_i\}$ and $\{\psi_j\}$ are the "i" and "j" vibration modes, respectively; the "*" and "T" symbols denote, respectively, the complex conjugate and the transpose of the eigenvectors. This way, the MAC computes the similarity between two vectors (whether real or complex) based on a degree of linearity varying from 0 to 1, where 0 indicates that there is no similarity between the vectors and 1 means that the vectors are completely similar. Moreover, it is acceptable to say that values above 0.80 (80%) indicate a high correlation whereas those below 0.20 (20%) present a poor correlation [45]. In this sense, the MAC is an interesting tool to evaluate how much the prestress level of cables may affect the mode shapes of the tensegrity module.

$$MAC_{ij} = \frac{\left|\{\psi_i\}^T\left\{\psi_j^*\right\}\right|^2}{\{\psi_i\}^T\{\psi_i^*\}\{\psi_j\}^T\{\psi_j^*\}} \tag{2}$$

Fig. 14a show the MAC matrix among the numerical vibration modes corresponding to the prestress level of 0.25% and 5%, which denotes a high similarity between the MAC values of the main diagonal and the off-diagonal terms approach zero. It means that such a difference in prestress level is not enough to change the behavior of the mode shapes. On the other hand, when the vibration modes corresponding to the extreme prestress level of 0.25% and 30% are compared to each other (Fig. 14b), the diagonals terms of the MAC matrix still display a high similarity (although slightly lower for the 1st, 2nd, 3rd and 5th modes), apart from the fourth mode, which approaches 0.7. Therefore, it indicates that this mode shape is prone to be affected by the prestress level.

Regarding the experimental results of the dynamic testing, as mentioned in Section 3.3, the structure was subjected to a free vibration test so that the force (input) and acceleration (output) signals were recorded in ARTeMIS program [46]. Based on the relationship between the latter and the former, these signals were thus converted to the frequency domain to obtain the average Frequency Response Functions (FRFs) related to the 14 impact points (the total FRFs measurements is equal to 14 × 10 impacts per node = 140). Subsequently, all FRFs were computed through the Complex Mode Indicator Function (CMIF) [49,50]. The CMIF is helpful to visualize the peaks corresponding to all the main natural frequencies in a single plot, since each peak of the curve is associated with a natural frequency and a mode of vibration. Thus, Fig. 15 shows the CMIF right after assembly (blue line), 4 days after (red line), 14 days after (yellow line) and, finally, 52 days after (magenta line). One can notice 25 peaks varying from 0.73 Hz to 48.34 Hz, as also listed in Table 9. From Fig. 15b, Table 9 and Fig. 16, it can be seen consistency among the experimental frequencies with respect to the tests performed on different days. It means that, although there may be a splitting of one peak into two, or even the opposite, that is, the union of two peaks into one, the frequency values do not change substantially. It is worth noting that a remarkable gap between the 19th and 20th peaks for all tests occurs (see Fig. 15b). This gap is also noticed between the 7th and 8th modes of the numerical model (see Table 7), which indicates a similar behavior of both experimental and numerical models. Besides, based on these results, one may infer that there was no relevant loss in the level of prestress applied to the structure during 52 days.

Finally, to find the experimental prestress level considering both numerical and experimental models – using the same approach in Section 4.1 – the dynamic relative errors (RE_d) between the numerical frequency and its nearest experimental neighbor were calculated using the following equation:

Table 10
Dynamic relative errors (RE_d) and sum of squares for different levels of prestress (S_0) varying from 0.25% to 30%.

S_0 (%)	M1	M2	M3	M4	M5	M6	M7	M8	M9	M10	$\Sigma(RE_d)^2$
0.25%	−0.08	−0.05	0.68	−0.02	0.01	−0.03	0.01	−0.04	−0.03	0.02	0.480
2.50%	−0.64	−0.62	−0.34	0.03	0.00	0.02	−0.02	−0.03	−0.01	0.02	0.910
5%	−0.49	−0.47	−0.06	0.09	−0.03	−0.01	0.04	−0.02	0.00	0.03	0.480
10%	−0.29	−0.26	0.00	−0.06	0.02	−0.06	0.00	0.00	0.03	0.04	0.160
15%	−0.13	−0.10	0.03	0.00	0.03	0.01	0.08	0.02	−0.05	0.05	0.041
20%	−0.01	0.03	−0.06	0.02	−0.03	0.07	0.16	0.04	−0.02	−0.06	0.043
25%	−0.02	0.02	0.01	0.01	0.03	0.14	−0.19	−0.04	0.00	−0.05	0.060
30%	−0.04	0.00	0.04	−0.04	0.09	0.20	−0.15	−0.02	0.03	−0.04	0.080

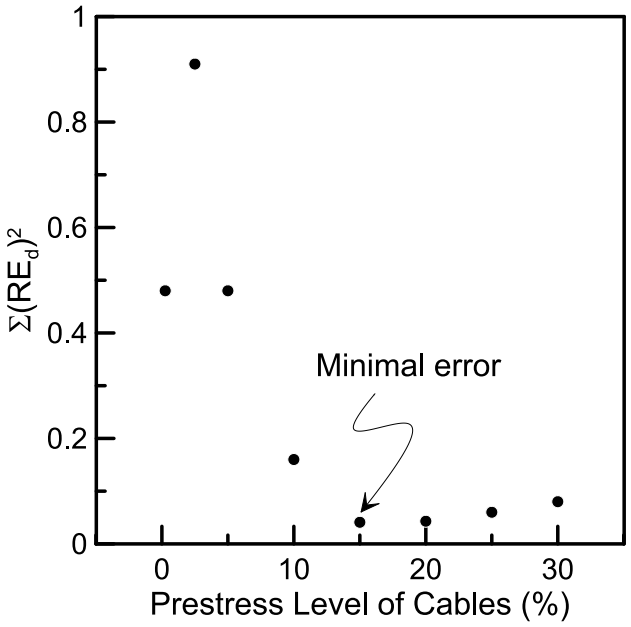

Fig. 17. Sum of squares of the dynamic relative error, $\Sigma(RE_d)^2$, for prestress level of cables varying from 0.25% to 30% and identification of the minimal error at 15%.

$$RE_d = \frac{numerical\ \ frequency\ \ (S_0) - experimental\ \ frequency}{experimental\ \ frequency} \tag{3}$$

The sum of squared errors for the first 10 modes of vibration of the tensegrity module was performed for prestresses ranging from 0.25% to 30%, as shown in Table 10. It is observed that prestress levels close to the extremes generated greater errors and intermediate levels (around 15%) showed smaller errors.

Plotting the curve $\sum(RE_d)^2$ vs. prestress levels (S_0), as illustrated in Fig. 17, it can be noted that prestresses between 0.25% and 10% resulted in considerably greater errors than those referring to levels of 15% to 30%. In fact, errors above 15% showed a very subtle variation, especially in the range of 15% and 20%. It can be seen from Fig. 17 that there is a local minimum between 12.5% and 17.5% of prestress, closer to 15% specifically. Accordingly, it is worth noting that a prestress level of 15% was also obtained in light of the static analysis (see Section 4.1). Therefore, this finding indicates a good agreement between both approaches and points to the robustness of the proposed methodology.

5. Conclusions

This paper aimed to design and investigate the level of prestress on a bio-based tensegrity module built using non-conventional materials, such as *Phyllostachys aurea* bamboo culms for the struts and sisal ropes (*Agave sisalana*) for the cable networks. Through the development of a fully reversible and biodegradable structural system, the developed scaled structure is deployable, ensuring rapid assembly and dismantling procedures. Therefore, the self-stress state of the structure was evaluated from an experimental and numerical approach, using both non-destructive static and dynamic analysis. Based on the analyzed data, the main conclusions of this study can be summarized as follows:

- Strut-cord joints were developed using a bamboo-sisal rope system, allowing for the end-of-life biodegradability of the joints and the structure as a whole. Thus, a fully bio-based tensegrity structure was reached without the utilization of metallic elements. In this sense, bamboo struts and sisal ropes showed appropriate physical and mechanical properties for the application in sustainable engineering structures.
- A novel nonlinear structural analysis software named Galileo, specially developed for bistable structures and tensegrities, was used. By computing the relative errors between numerical and experimental compressive static stresses, the level of prestress acting on the structure right after the assembly is close to 15%. Concurrently, the evaluation of the relative errors based on the natural frequencies of the structure allowed the authors to infer that the level of prestress applied to the module right after assembly is also approximately 15%, which indicates a good agreement between them and points to the robustness of the proposed methodology. The prestress results equal to 15% is relatively close to the expected value, since initially the structure was designed to have a theoretical prestress of 5%. This difference is possibly due to construction aspects, that might have affected the final level of prestress.
- There was no relevant loss in the level of prestress applied to the structure during 52 days under laboratory conditions since the experimental natural frequencies did not change substantially, which is important data for the application of sisal ropes for cable nets in bio-based tensegrity structures.
- The application of full-scale bio-based tensegrity systems should be further developed and investigated under environmental conditions, i.e. external loads that represent its use as footbridges; consider modeling tensegrity bamboo structures with curved struts in a regime of large displacements, including their axial imperfections and eccentricities due to the superposition of the joints, broadening the boundaries of the field in order to reach sustainability within Civil Engineering.

Data availability statement

The raw data required to reproduce the findings are available from the corresponding author, upon reasonable request.

CRediT authorship contribution statement

Nathalia B. de Albuquerque: Conceptualization, Methodology, Formal analysis, Investigation, Writing – original draft. **Cássio M.R. Gaspar:** Conceptualization, Methodology, Investigation, Supervision, Writing – original draft, Writing – review & editing. **Mario Seixas:** Conceptualization, Investigation, Writing – review & editing. **Murillo V. B. Santana:** Software, Investigation, Writing – review & editing. **Daniel**

C.T. Cardoso: Conceptualization, Supervision, Writing – review & editing.

Declaration of Competing Interest

The authors declare that they have no known competing financial interests or personal relationships that could have appeared to influence the work reported in this paper.

Acknowledgments

All tests were performed in the Laboratory of Structures and Materials of the Pontifical Catholic University of Rio de Janeiro. This study was financed in part by the Coordenação de Aperfeiçoamento de Pessoal de Nível Superior – CAPES, Finance Code 001 – and by Brazilian agencies FAPERJ and CNPq.

References

[1] Motro R. Tensegrity - Structural Systems for the Future. 1st Ed. Kogan Page; 2003.
[2] Motro R. Tensegrity Systems: The State of the Art. Int J Sp Struct 1992;7:75–83. https://doi.org/10.1177/026635119200700201.
[3] Snelson K. The Art of Tensegrity. Int J Sp Struct 2012;27:71–80. https://doi.org/10.1260/0266-3511.27.2-3.71.
[4] Fuller RB. Synergetics: Explorations in the geometry of thinking. MacMillan Publishing Company; 1976.
[5] Oliveira MC, Skelton RE. In: Oliveira MC, Skelton RE, editors. Tensegrity systems. New York, NY: Springer US; 2009.
[6] Sultan C. Chapter 2 Tensegrity: 60 Years of Art, Science, and Engineering. vol. 43. 1st ed. Elsevier Inc.; 2009. https://doi.org/10.1016/S0065-2156(09)43002-3.
[7] Wang Y, Xu X, Luo Y. Minimal mass design of active tensegrity structures. Eng Struct 2021;234:111965. https://doi.org/10.1016/j.engstruct.2021.111965.
[8] Mirats Tur JM, Juan SH. Tensegrity frameworks: Dynamic analysis review and open problems. Mech Mach Theory 2009;44:1–18. https://doi.org/10.1016/j.mechmachtheory.2008.06.008.
[9] Gilewski W, Kłosowska J, Obara P. Applications of tensegrity structures in civil engineering. Procedia Eng 2015;111:242–8. https://doi.org/10.1016/j.proeng.2015.07.084.
[10] Seixas M, Bina J, Stoffel P, Ripper JL, Moreira LE, Ghavami K. Active bending and tensile pantographic bamboo hybrid amphitheater structure. J Int Assoc Shell Spat Struct 2017;58:239–52. https://doi.org/10.20898/j.iass.2017.193.872.
[11] Micheletti A. Modular Tensegrity Structures: The "Tor Vergata" Footbridge. Mech Model Methods Civ Eng 2012:375–84. https://doi.org/10.1007/978-3-642-24638-8_25.
[12] Feron J, Boucher L, Denoël V, Latteur P. Optimization of Footbridges Composed of Prismatic Tensegrity Modules. J Bridg Eng 2019;24:04019112. https://doi.org/10.1061/(asce)be.1943-5592.0001438.
[13] Gao S, Xu X, Luo Y. Re-study on tensegrity footbridges based on ring modules. Adv Struct Eng 2020;23:898–910. https://doi.org/10.1177/1369433219886080.
[14] Gómez-Jáuregui V, Arias R, Otero C, Manchado C. Novel technique for obtaining double-layer tensegrity grids. Int J Sp Struct 2012;27:155–66. https://doi.org/10.1260/0266-3511.27.2-3.155.
[15] Rhode-Barbarigos L, Hadj Ali NB, Motro R, Smith IFC. Designing tensegrity modules for pedestrian bridges. Eng Struct 2010;32:1158–67. https://doi.org/10.1016/j.engstruct.2009.12.042.
[16] Rhode-Barbarigos L, Ali NBH, Motro R, Smith IFC. Design aspects of a deployable tensegrity-hollow-rope footbridge. Int J Sp Struct 2012;27:81–95. https://doi.org/10.1260/0266-3511.27.2-3.81.
[17] Bel Hadj Ali N, Rhode-Barbarigos L, Pascual Albi AA, Smith IFC. Design optimization and dynamic analysis of a tensegrity-based footbridge. Eng Struct 2010;32:3650–9. https://doi.org/10.1016/j.engstruct.2010.08.009.
[18] Kebiche K, Kazi-Aoual MN, Motro R. Geometrical non-linear analysis of tensegrity systems. Eng Struct 1999;21:864–76. https://doi.org/10.1016/S0141-0296(98)00014-5.
[19] Ben Kahla N, Kebiche K. Nonlinear elastoplastic analysis of tensegrity systems. Eng Struct 2000;22:1552–66. https://doi.org/10.1016/S0141-0296(99)00088-7.
[20] Tran HC, Lee J. Geometric and material nonlinear analysis of tensegrity structures. Acta Mech Sin Xuebao 2011;27:938–49. https://doi.org/10.1007/s10409-011-0520-2.
[21] Murakami H. Static and dynamic analyses of tensegrity structures. Part II. Quasi-static analysis. Int J Solids Struct 2001;38:3615–29. https://doi.org/10.1016/S0020-7683(00)00233-X.
[22] Rhode-Barbarigos L, Jain H, Kripakaran P, Smith IFC. Design of tensegrity structures using parametric analysis and stochastic search. Eng Comput 2010;26:193–203. https://doi.org/10.1007/s00366-009-0154-1.
[23] Ashwear N, Eriksson A. Natural frequencies describe the pre-stress in tensegrity structures. Comput Struct 2014;138:162–71. https://doi.org/10.1016/j.compstruc.2014.01.020.
[24] Faroughi S, Tur JMM. Vibration properties in the design of tensegrity structure. JVC/Journal Vib Control 2015;21:611–24. https://doi.org/10.1177/1077546313493310.
[25] Ashwear N, Eriksson A. Vibration health monitoring for tensegrity structures. Mech Syst Signal Process 2017;85:625–37. https://doi.org/10.1016/j.ymssp.2016.08.039.
[26] Chen Y, Sun Q, Feng J. Improved Form-Finding of Tensegrity Structures Using Blocks of Symmetry-Adapted Force Density Matrix. J Struct Eng 2018;144:04018174. https://doi.org/10.1061/(asce)st.1943-541x.0002172.
[27] Chen Y, Feng J, Lv H, Sun Q. Symmetry representations and elastic redundancy for members of tensegrity structures. Compos Struct 2018;203:672–80. https://doi.org/10.1016/j.compstruct.2018.07.044.
[28] Seixas M, Moreira LE, Stoffel P, Bina J, Ripper JLM, Ferreira JL, et al. Analysis of a self-supporting bamboo structure with flexible joints. Int J Sp Struct 2021;36(2):137–51. https://doi.org/10.1177/09560599211001660.
[29] Tran HC, Lee J. Initial self-stress design of tensegrity grid structures. Comput Struct 2010;88:558–66. https://doi.org/10.1016/j.compstruc.2010.01.011.
[30] Rhode-Barbarigos L, Schulin C, Ali NBH, Motro R, Smith IFC. Mechanism-Based Approach for the Deployment of a Tensegrity-Ring Module. J Struct Eng 2012;138:539–48. https://doi.org/10.1061/(asce)st.1943-541x.0000491.
[31] Fraddosio A, Pavone G, Piccioni MD. Minimal mass and self-stress analysis for innovative V-Expander tensegrity cells. Compos Struct 2019;209:754–74. https://doi.org/10.1016/j.compstruct.2018.10.108.
[32] Korkmaz S, Ali NBH, Smith IFC. Configuration of control system for damage tolerance of a tensegrity bridge. Adv Eng Informatics 2012;26:145–55. https://doi.org/10.1016/j.aei.2011.10.002.
[33] Satyanarayana KG, Guimarães JL, Wypych F. Studies on lignocellulosic fibers of Brazil. Part I: Source, production, morphology, properties and applications. Compos Part A Appl Sci Manuf 2007;38:1694–709. https://doi.org/10.1016/j.compositesa.2007.02.006.
[34] Yan L, Kasal B, Huang L. A review of recent research on the use of cellulosic fibres, their fibre fabric reinforced cementitious, geo-polymer and polymer composites in civil engineering. Compos Part B Eng 2016;92:94–132. https://doi.org/10.1016/j.compositesb.2016.02.002.
[35] ISO 22157-1:2004. Bamboo — Determination of physical and mechanical properties — Part 1: Requirements. Switzerland: International Organization for Standardization; 2004.
[36] ISO 22157:2019. Bamboo structures — Determination of physical and mechanical properties of bamboo culms — Test methods. Switzerland: International Organization for Standardization; 2019.
[37] TDC8(5628)P3. Textiles – Ropes Specifications: Part 1. Ropes made from natural fibres. Tanzania Standard; 2018.
[38] Albuquerque NB de. Construction and mechanical behavior of a Tensegrity Pedestrian Bridge built with natural materials [MSc dissertation in Civil Engineering: in portuguese]. Pontifical Catholic University of Rio de Janeiro (PUC-Rio); 2020. https://doi.org/10.17771/PUCRio.acad.50792.
[39] Kittner C, Quimby SR. Compression-tension strut-cord units for tensile-integrity structures. 4,731,962; 1988.
[40] SANTANA MVB. Tailored Corotational Formulations for the Nonlinear Static and Dynamic Analysis of Bistable Structures [Ph.D. thesis in Civil Engineering]. Pontifical Catholic University of Rio de Janeiro (PUC-Rio); 2019.
[41] Fraternali F, Bilotti G. Nonlinear elastic stress analysis in curved composite beams. Comput Struct 1997;62:837–59. https://doi.org/10.1016/S0045-7949(96)00301-X.
[42] Fraternali F, Spadea S, Ascione L. Buckling behavior of curved composite beams with different elastic response in tension and compression. Compos Struct 2013;100:280–9. https://doi.org/10.1016/j.compstruct.2012.12.021.
[43] Rodríguez MCG. Design framework for bamboo culms - A study of bamboo reciprocal structures [Ph.D. thesis in Civil Engineering]. University College London; 2019.
[44] Brandt A. Noise and vibration analysis: signal analysis and experimental procedures. John Wiley & Sons; 2011.
[45] Ewins DJ. Modal Testing. Theory, practice and application. 2nd ed. Wiley; 2000.
[46] Structural-Vibration-Solutions. ARTeMIS Modal Pro 6.0; 2019.
[47] Armandei M, Darwish IF, Ghavami K. Experimental study on variation of mechanical properties of a cantilever beam of bamboo. Constr Build Mater 2015;101:784–90. https://doi.org/10.1016/j.conbuildmat.2015.10.078.
[48] Divós F, Tanaka T. Relation Between Static and Dynamic Modulus of Elasticity of Wood. Acta Silv Lign Hung 2005;1:105–10.
[49] Avitabile P. Modal testing: A practitioner's guide. John Wiley & Sons; 2018.
[50] Allemang RJ, Brown DL. A complete review of the complex mode indicator function (CMIF) with applications. Proc ISMA2006 Int Conf Noise Vib Eng 2006;6:3209–46.